Progress In Electromagnetics Research, Vol. 138, 41–63, 2013

AN EXTENDED FREQUENCY SCALING ALGORITHM FOR HIGH SQUINT SPOTLIGHT AIRBORNE SAR

Weihua Zuo[1, 2, *], Yiming Pi[1], and Rui Min[1]

[1]School of Electronic Engineering, University of Electronic Science and Technology of China, Chengdu, Sichuan 611731, People's Republic of China

[2]Physics and Information Engineering Department, Huaihua University, Huaihua, Hunan 418000, People's Republic of China

Abstract—In high squint spotlight mode SAR, the coupling of the range and azimuth is very serious, which brings challenges to the imaging. In this paper, an extended frequency scaling algorithm is proposed, in which the range migration correction is divided into two steps. Firstly the range walk correction is implemented in 2D time domain. In the second step, the residual range migration is corrected by the frequency scaling and bulk shift operations. Though the second range compression does not consider the range space variance, the range compression is precise. In the azimuth compression, because of the range walk correction, the azimuth modulation frequency rate becomes dependent on the azimuth position. In order to equalize the azimuth modulation frequency rate, the azimuth nonlinear chirp scaling method is involved to remove the dependence. The simulation experiments verify the validity of the proposed algorithm. The comparison of the imaging quality among traditional frequency scaling algorithm, nonlinear frequency scaling algorithm and the proposed method indicates the proposed method is more suitable for the high squint spotlight SAR.

1. INTRODUCTION

Synthetic aperture radar (SAR) can obtain high resolution microwave images of the observed area in all-time and all-weather conditions. Spotlight mode of SAR can get the super resolution images of the target scene [1], 0.1 m [2] for airborne platform and 1 m [3] for spaceborne

Received 3 January 2013, Accepted 4 March 2013, Scheduled 15 March 2013

* Corresponding author: Weihua Zuo (kingso801021@163.com).

platform, which makes it a very attractive and active research field in remote sensing.

When SAR works in the spotlight mode, the beam is steered properly to illuminate the same scene. The steering of the antenna results in a longer synthetic time and aperture than the stripmap mode, which provides the probability of a finer azimuth resolution than the ideal azimuth resolution gotten in stripmap mode. In order to get the equivalent range resolution, very wide bandwidth pulses need to be transmitted and received, which will make the receiving and sampling very difficult for the A/D devices. There are two solutions to conquer this difficulty: the first one is to transmit narrow bandwidth stepped chirps [4–6]. The second is the dechirp-receiving method [1]. It is suitable for the small scene. Because the sizes of the observed scenes of the spotlight SAR are small in most situations, the dechirp-receiving method is considered in this paper.

High squint angle can improve the flexibility and extend application fields of SAR. But when SAR works under high squint angle, the range cell migration (RCM) amount of the target is much huger than that of the corresponding broadside. Moreover because the spotlight mode has longer synthetic aperture and time, the huge RCM amount of the high squint spotlight mode results in the serious coupling of the range and the azimuth, which brings great challenges to the focusing.

The imaging algorithms for spotlight SAR include the polar format algorithm (PFA) [1, 7, 8], the range migration algorithm (RMA) [1, 9–11], the chirp scaling algorithm (CSA) [12], the two step focusing approach (TSFA) [13–15] and the frequency scaling algorithm (FSA) [16, 17] and so on. In PFA, the echo signal is dechirped with a reference function whose reference range is the instantaneous range of the scene center, which can be viewed as dechirp operation both in the range direction and in the azimuth direction. The PFA is able to handle high squint situation. The RMA reconstructs the 2D spectrum by Stotle interpolation. Thus the RMA can process the high squint data too. But the RMA requires that the echo signal should not be dechirp-received, i.e., the echo signal before converted to wavenumber domain by 2D FFT should be in chirp form. Moreover in the PFA and RMA, the interpolation operations are unavoidable, which results in the low-efficiency of them. The CSA and TSFA can be used to process the spotlight SAR data, while require a chirp-form return signal too.

The FSA was proposed in [16], which brought up the frequency scaling theory. It can directly process dechirp-received signal. Moreover only fast Fourier transform (FFT) and complex multiplication operations are required, which improve the efficiency of

FSA in contrast to PFA and RMA. But in FSA the space variance of the second range compression (SRC) term is neglected, which makes the FSA unable to process high squint spotlight data. The literature [18], referring to the nonlinear chirp scaling algorithm (NCSA) [19, 20], proposed the nonlinear frequency scaling algorithm (NFSA), which can improve the high squint data processing ability. But with the increase of the squint angle, the image quality decreases obviously.

In order to improve the high squint angle data processing ability, this paper proposes an extended frequency scaling algorithm (EFSA). In the EFSA the residual video phase (RVP) generated in the dechirp-receiving is compensated in the preprocessing step, which is different from that of FSA. Then a range walk correction is implemented in 2D time domain, which does not exist in FSA and NFSA at all. Thus the whole processing steps of EFSA are in fact quite different from those of FSA and NFSA. Because it takes advantage of the theory of frequency scaling, the proposed algorithm is called EFSA here.

The paper is organized as follows. In Section 2 the geometry and signal mode of the high squint spotlight mode are described. The EFSA is proposed in the Section 3, which includes the analysis and derivation in detail. Section 4 gives the results of the simulation experiments. Section 5 concludes the whole paper.

2. SIGNAL MODE OF HIGH SQUINT SPOTLIGHT SAR

The geometry of high squint spotlight SAR is shown in Fig. 1. The platform travels along the trajectory that is parallel with the azimuth direction x. The synthetic aperture center locates at O'. During the flight, the radar beam is constantly steered to illuminate the scene center C, which is set as the origin of the azimuth direction. The squint angle θ_s is the angle between the antenna pointing direction at O' and the orthogonal direction to the flight trajectory. The azimuth position of point target P is x_p. The shortest slant range between P

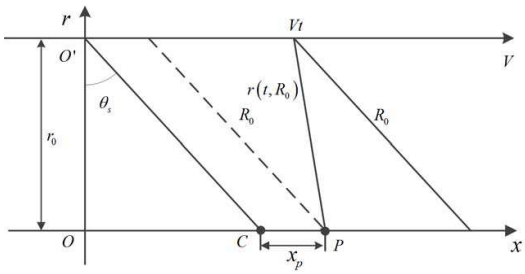

Figure 1. Geometry of high squint spotlight SAR.

and the platform is r_0 and the slant range between them in the squint angle direction is $R_0 = \frac{r_0}{\cos\theta_s}$.

According to the geometry, the instantaneous slant range $r(t, R_0)$ of P is as (1), in which t is the slow time.

$$\begin{aligned} r(t, R_0) &= \sqrt{R_0^2 + (Vt - x_p)^2 - 2R_0 (Vt - x_p) \sin\theta_s} \\ &\approx \sqrt{R_0^2 + V^2 \cos^2\theta_s \left(t - \frac{x_p}{V}\right)^2} - V \sin\theta_s \left(t - \frac{x_p}{V}\right) \\ &\quad + \frac{V^3 \cos^2\theta_s \sin\theta_s}{2R_0^2} \left(t - \frac{x_p}{V}\right)^3 \end{aligned} \tag{1}$$

The second and the third lines of Equation (1) is the approximation of $r(t, R_0)$ that only omits the odd order terms whose orders are higher than 5. The second term in the second line of equation represents the range walk, which is independent on the target.

The dechirp-received signal of P is as (2), in which τ is the fast time; K_s is the frequency modulation rate; f_c is the carry frequency; $\lambda = \frac{c}{f_c}$ is the wave length; r_c is the shortest slant range of the scene center; $R_c = \frac{r_c}{\cos\theta_s}$ is the distance between the scene center and the synthetic aperture center.

$$\begin{aligned} ss_1(\tau, t) = A &\text{rect}\left(\frac{\tau - \frac{2r(t,R_0)}{c}}{T_p}\right) \text{rect}\left(\frac{t}{T_a}\right) \\ &\cdot \exp\left\{-j\frac{4\pi K_s}{c}\left(\tau - \frac{2R_c}{c}\right)(r(t, R_0) - R_c)\right\} \\ &\exp\left\{-j\frac{4\pi}{\lambda}(r(t, R_0) - R_c)\right\} \exp\left\{j\frac{4\pi K_s}{c^2}(r(t, R_0) - R_c)^2\right\} \end{aligned} \tag{2}$$

The last phase term of (2) is the residual video phase (RVP) that must be compensated.

3. THE EXTENDED FREQUENCY SCALING ALGORITHM BASED ON THE RANGE WALK CORRECTION IN TIME DOMAIN

In EFSA, the range migration correction is accomplished by two steps. They are the range walk correction (RWC) and the range curvature correction respectively. Because of RWC, the azimuth modulation rate varies with the azimuth time. The azimuth nonlinear chirp scaling (ANCS) method will be involved to equalize the azimuth modulation rate. The processing steps of EFSA are quite different from that of FSA and NFSA. This section will give the derivation and analysis in detail.

3.1. Preprocessing: RVP Correction

The RVP correction is finished in the preprocessing step. It is called deskew operation, which is implemented in the fast time frequency domain. Convert (2) to fast time frequency domain and multiply it with the deskew function as (3):

$$H_{deskew}\left(f_r\right) = \exp\left(-j\frac{\pi}{K_s}f_r^2\right) \tag{3}$$

The deskewed signal is as (4) after converting back to the time domain.

$$\begin{aligned} ss_2(\tau,t) = & A\text{rect}\left(\frac{\tau-\frac{2R_c}{c}}{T_p}\right)\text{rect}\left(\frac{t}{T_a}\right) \\ & \cdot\exp\left\{-j\left[\frac{4\pi}{\lambda}+\frac{4\pi K_s}{c}\left(\tau-\frac{2R_c}{c}\right)\right]\left(r\left(t,R_0\right)-R_c\right)\right\} \end{aligned} \tag{4}$$

After this operation, the range envelop of (4) has been centered at the fast time delay $\frac{2R_c}{c}$ and the RVP term in (2) is removed.

3.2. Range Walk Correction in Time Domain

According to the approximation of $r(t, R_0)$ in (1), the RWC function can be set as (5).

$$H_{RWC}\left(\tau,t\right) = \exp\left\{-j\left[\frac{4\pi}{\lambda}+\frac{4\pi K_s}{c}\left(\tau-\frac{2R_c}{c}\right)\right]V\sin\theta_s t\right\} \tag{5}$$

After multiplying (4) with (5), the signal after RWC is as (6), in which $r_1(t, R_0) \approx \sqrt{R_0^2 + V^2\cos^2\theta_s(t-\frac{x_p}{V})^2}$.

$$\begin{aligned} ss_3(\tau,t) \approx & A\text{rect}\left(\frac{\tau-\frac{2R_c}{c}}{T_p}\right)\text{rect}\left(\frac{t}{T_a}\right) \\ & \cdot\exp\left\{-j\left[\frac{4\pi}{\lambda}+\frac{4\pi K_s}{c}\left(\tau-\frac{2R_c}{c}\right)\right]\left(x_p\sin\theta_s-R_c\right)\right\} \\ & \cdot\exp\left\{-j\left[\frac{4\pi}{\lambda}+\frac{4\pi K_s}{c}\left(\tau-\frac{2R_c}{c}\right)\right]r_1\left(t,R_0\right)\right\} \\ & \cdot\exp\left\{-j\left[\frac{4\pi}{\lambda}+\frac{4\pi K_s}{c}\left(\tau-\frac{2R_c}{c}\right)\right]\frac{V^3\cos^2\theta_s\sin\theta_s}{2R_0^2}\left(t-\frac{x_p}{V}\right)^3\right\} \end{aligned} \tag{6}$$

The expression (6) is like the echo signal gotten in the broadside situation. And in fact, the RWC expression in (5) can be viewed

as the precise Doppler center frequency compensation. The azimuth frequency is moved to the low-pass band as shown in (7), in which f_{dc} is the Doppler center frequency.

$$f_a \in \left[f_{dc} - \frac{PRF}{2},\, f_{dc} + \frac{PRF}{2}\right] \rightarrow f_a \in \left[-\frac{PRF}{2}, \frac{PRF}{2}\right] \tag{7}$$

Using the principle of station phase (POSP) and omitting the third and higher order terms, (6) can be converted to the RD domain as (8).

$$\begin{aligned} sS_4(\tau, f_a) = A\mathrm{rect}&\left(\frac{\tau - \frac{2R_c}{c}}{T_p}\right)\mathrm{rect}\left(\frac{t}{T_a}\right)\exp\left(-j2\pi f_a\frac{x_p}{V}\right) \\ &\cdot\exp\left\{-j\left[\frac{4\pi}{\lambda} + \frac{4\pi K_s}{c}\left(\tau - \frac{2R_c}{c}\right)\right](x_p\sin\theta_s - R_c)\right\} \\ &\cdot\exp\left\{-j\frac{4\pi R_0}{\lambda}\sqrt{\left[\frac{\lambda K_s}{c}\left(\tau - \frac{2R_c}{c}\right)+1\right]^2 - \left(\frac{\lambda f_a}{2V\cos\theta_s}\right)^2}\right\} \\ &\cdot\exp\left\{j\frac{2\pi R_0\tan\theta_s}{\lambda}\frac{\left[1+\frac{\lambda K_s}{c}\left(\tau - \frac{2R_c}{c}\right)\right]\left(\frac{\lambda f_a}{2V\cos\theta_s}\right)^3}{\left[\left[1+\frac{\lambda K_s}{c}\left(\tau - \frac{2R_c}{c}\right)\right]^2 - \left(\frac{\lambda f_a}{2V\cos\theta_s}\right)^2\right]^{3/2}}\right\} \end{aligned} \tag{8}$$

In order to analyze (8) in detail, the phase of it is expanded in Taylor series at $\tau = \frac{2R_c}{c}$ as (9), in which $D(f_a) = \sqrt{1 - (\frac{\lambda f_a}{2V\cos\theta_s})^2}$ and the coefficients are as (10).

$$\begin{aligned} \varphi_1(\tau, f_a; R_0) = &-2\pi f_a\frac{x_p}{V} + \phi_0(f_a, R_0) + \phi_1(f_a, R_0)\left(\tau - \frac{2R_c}{c}\right) \\ &+\phi_2(f_a, R_0)\left(\tau - \frac{2R_c}{c}\right)^2 + \phi_3(f_a, R_0)\left(\tau - \frac{2R_c}{c}\right)^3 \end{aligned} \tag{9}$$

$$\begin{cases} \phi_0(f_a, R_0) = -\frac{4\pi R_0 D(f_a)}{\lambda} + \frac{2\pi R_0\tan\theta_s\left(1-D^2(f_a)\right)^{3/2}}{\lambda D^3(f_a)} \\ \phi_1(f_a, R_0) = -\frac{4\pi K_s}{c}\left(\frac{R_0}{D(f_a)} - \frac{R_0\tan\theta_s\left[1-D^2(f_a)\right]^{3/2}\left(D^2(f_a)-3\right)}{2D^5(f_a)}\right. \\ \qquad\qquad \left. -R_c + x_p\sin\theta_s\right) \triangleq 2\pi f_s \\ \phi_2(f_a, R_0) = \frac{2\pi\lambda R_0 K_s^2}{c^2}\frac{1-D^2(f_a)}{D^3(f_a)} \\ \qquad\qquad + \frac{3\pi\lambda K_s^2 R_0\tan\theta_s\left[1-D^2(f_a)\right]^{3/2}}{c^2}\frac{5-3D^2(f_a)}{D^7(f_a)} \triangleq \pi K_m \\ \phi_3(f_a, R_0) = -\frac{2\pi\lambda^2 R_0 K_s^3\left(1-D^2(f_a)\right)}{c^3 D^5(f_a)} \\ \qquad\qquad + \frac{\pi\lambda^2 R_0 K_s^3\tan\theta_s\left[1-D^2(f_a)\right]^{3/2}}{c^3}\frac{-3D^4(f_a)+30D^2(f_a)-35}{D^9(f_a)} \end{cases} \tag{10}$$

In (10), $\phi_0(f_a, R_0)$ represents the azimuth modulation. $\phi_1(f_a, R_0)$ is the residual range migration, i.e., the range curvature terms, which is dependent on R_0. The quadratic term coefficient $\phi_2(f_a, R_0)$ represents the SRC. $\phi_3(f_a, R_0)$ is the coefficient of the cubic phase term.

3.3. Frequency Scaling Operation

Based on the analysis in Subsection 3.2, it is known that the range curvature is space variant. In order to correct the range curvatures of all targets once, the space variance must be removed, which can be finished with the frequency scaling (FS) operation that will be implemented in wave number domain. With the approximation of the phase, (8) will be converted to wave number domain with POSP and the expression is as (11). When using POSP, the cubic phase term of (9) is omitted, because after RWC it is very small. For simplicity, the range and the azimuth envelop are neglected in (11).

$$\begin{aligned} SS_5(f_r, f_a) = & \exp\left(-j2\pi f_a \frac{x_p}{V}\right) \exp\left\{j\phi_0\left(f_a, R_0\right)\right\} \\ & \cdot \exp\left\{-j\frac{\pi}{K_m}\left(f_r - f_s\right)^2\right\} \exp\left\{-j\frac{4\pi R_c}{c} f_r\right\} \end{aligned} \quad (11)$$

In (11):

$$\begin{cases} K_m \triangleq \frac{2\lambda R_0 K_s^2}{c^2} \frac{1-D^2(f_a)}{D^3(f_a)} + \frac{3\lambda K_s^2 R_0 \tan\theta_s \left[1-D^2(f_a)\right]^{3/2}}{c^2} \frac{5-3D^2(f_a)}{D^7(f_a)} \\ f_s \triangleq -\frac{2K_s}{c}\left[R_0\alpha\left(f_a\right) + x_p \sin\theta_s - R_c\right] \end{cases}$$

The $\alpha(f_a) = \frac{1}{D(f_a)} - \tan\theta_s[1 - D^2(f_a)]^{3/2} \frac{D^2(f_a)-3}{2D^5(f_a)}$ is the range migration factor of point target P. From f_s, it is found that the position of P in fast time frequency domain is dependent on R_0, f_a and θ_s, which means it is space variant.

The FS function is as (12), in which $f_{ref} = -\frac{2K_s}{c}[R_c\alpha(f_a) - R_c]$. It means the scene center target is selected as the reference target.

$$H_{FS}\left(f_a, f_r\right) = \exp\left\{-j\frac{\pi}{K_{mref}}\left(\alpha\left(f_a\right) - 1\right)\left(f_r - f_{ref}\right)^2\right\} \quad (12)$$

In (12) $K_{mref} = K_m(f_a, R_c)$ is used to substitute K_m to give the FS function. The approximation will result in the phase error. But it can be ignored. After multiplying (11) with (12), the signal after FS operation is as (13).

$$\begin{aligned} SS_6(f_r, f_a) = & \exp\left\{j\phi_0\left(f_a, R_0\right)\right\} \cdot \exp\left\{-j\frac{\pi}{K_{mref}}\alpha\left(f_a\right)\left(f_r - f_{fs}\right)^2\right\} \\ & \exp\left\{-j\frac{4\pi R_c}{c} f_r\right\} \exp\left\{j\phi_{res}\left(f_a, R_0\right)\right\} \end{aligned} \quad (13)$$

In (13), $\phi_{res}(f_a, R_0)$ is the residual phase generated by the FS operation as (14), which must be compensated.

$$\begin{aligned}&\phi_{res}\left(f_a, R_0\right)\\&=\exp\left\{-j\frac{\pi}{K_{mref}}\alpha\left(f_a\right)\left(\alpha\left(f_a\right)-1\right)\left[K_s\left(\frac{2R_0}{c}-\frac{2R_c}{c}\right)+\frac{x_p\sin\theta_s}{\alpha\left(f_a\right)}\right]^2\right\}\end{aligned} \quad (14)$$

From (13) it is found that all the targets have the same range migration, thus they can be corrected once.

3.4. Second Range Compression and Bulk Shift

The second range compression and the bulk shift operations will fulfill the range compression and the range curvature correction in RD domain. Before these two operations, (13) should be converted to RD domain as (15).

$$\begin{aligned}sS_7(\tau, f_a)=&\exp\left(-j2\pi f_a\frac{x_p}{V}\right)\exp\left\{j\phi_0\left(f_a, R_0\right)\right\}\\&\cdot\exp\left\{j\frac{\pi K_{mref}}{\alpha\left(f_a\right)}\left(\tau-\frac{2R_c}{c}\right)^2\right\}\\&\exp\left(j2\pi f_{fs}\left(\tau-\frac{2R_c}{c}\right)\right)\exp\left\{j\phi_{res}\left(f_a, R_0\right)\right\}\end{aligned} \quad (15)$$

According to (15), the SRC and bulk shift transform function should be as (16).

$$\begin{aligned}H_{SRC+BV}\left(\tau, f_a\right)=&\exp\left\{-j\frac{\pi K_{mref}}{\alpha\left(f_a\right)}\left(\tau-\frac{2R_c}{c}\right)^2\right\}\\&\exp\left\{j\frac{4\pi K_s}{c}R_c\left(\alpha\left(f_a\right)-1\right)\left(\tau-\frac{2R_c}{c}\right)\right\}\end{aligned} \quad (16)$$

After multiplying (15) with (16) and converting the multiplication results to the range frequency domain, (17) is gotten.

$$\begin{aligned}SS_8(f_r, f_a)=&\sin c\left\{B_r\left[f_r+\frac{2K_s}{c}\left(R_0+x_p\sin\theta_s-R_c\right)\right]\right\}\\&\cdot\exp\left(-j2\pi f_a\frac{x_p}{V}\right)\exp\left\{j\phi_0\left(f_a, R_0\right)\right\}\exp\left\{j\phi_{res}\left(f_a, R_0\right)\right\}\end{aligned} \quad (17)$$

The residual phase compensation function is as (18).

$$H_{rpc}\left(f_a, R_0\right)=\exp\left\{j\frac{\pi}{K_{mref}}\frac{\alpha\left(f_a\right)-1}{\alpha\left(f_a\right)}\left(f_s-f_{ref}\right)^2\right\} \quad (18)$$

After the residual phase compensation, the final range compressed signal is as (19).

$$SS_9(f_r, f_a) = \sin c\left\{B_r\left[f_r + \frac{2K_s}{c}\left(R_0 + x_p \sin\theta_s - R_c\right)\right]\right\} \cdot \exp\left(-j2\pi f_a \frac{x_p}{V}\right) \exp\left\{j\phi_0\left(f_a, R_0\right)\right\} \quad (19)$$

From (19), it is found that the target location is $f_r = -\frac{2K_s}{c}(R_0 + x_p \sin\theta_s - R_c)$, corresponding to the slant range $R \triangleq R_0 + x_p \sin\theta_s \triangleq R_0 + Vt_d \sin\theta_s$.

3.5. Analysis of Azimuth Compression

After the range compression, the azimuth phase terms can be summed in (20).

$$\begin{aligned}\varphi_2(f_a, R_0) &= -\frac{4\pi R_0 D\left(f_a\right)}{\lambda} + \frac{2\pi R_0 \tan\theta_s \left(1 - D^2\left(f_a\right)\right)^{3/2}}{\lambda D^3\left(f_a\right)} - 2\pi f_a \frac{x_p}{V} \\ &\approx -\frac{4\pi R_0}{\lambda} - 2\pi f_a \frac{x_p}{V} + \frac{\pi\lambda R_0}{2V^2 \cos^2\theta_s} f_a^2 + \frac{\pi\lambda^2 R_0 \sin\theta_s}{4V^3 \cos^4\theta_s} f_a^3 + \ldots \quad (20)\end{aligned}$$

From (20), the azimuth modulation rate is $K_a = -\frac{2V^2\cos^2\theta_s}{\lambda R_0}$, which is dependent on R_0. But after the range compression, the azimuth modulation rate must be calculated by R [21, 22], which means in order to finish the azimuth compression, K_a must vary with the azimuth time. Thus the traditional azimuth compression method fails in this situation. The literature [23] equalizes the azimuth modulation rate by introducing an azimuth perturbation function, while it will result in distortion in the final images and the necessary interpolation operation makes the method inefficient. The references [21, 22] introduce another solving strategy named ANCS to correct the space variance of K_a, in which only complex multiplication and FFT operations are needed. In EFSA the ANCS method will be involved in the azimuth compression.

3.6. Azimuth Cubic Phase Filtering

In the ANCS method, the cubic phase of (20) must be filtered, because in high squint angle it is too large to be ignored. Let the cubic phase filter be as (21), in which $Y(R)$ is undetermined.

$$H_{3ord}(f_r, f_a) = \exp\left(j\frac{2\pi}{3} Y\left(R\right) f_a^3\right) \quad (21)$$

Multiplying (21) with (20), the filtered signal is gotten as (22), in which $Y_m(R) = Y(R) + \frac{3}{2\pi}\phi_3(R, t_d)$. Because the space variance of the cubic phase can be ignored, $\phi_3(R_0, t_d)$ can be substituted by $\phi_3(R, 0)$.

$$SS_{10}(f_r, f_a) = Ap_r(f_r) \exp\left(-j2\pi f_a \frac{x_p}{V}\right) \exp\left(-j\frac{\pi}{K_a} f_a^2\right) \exp\left(j\frac{2\pi}{3} Y_m(R) f_a^3\right) \quad (22)$$

After converting (22) to the azimuth time domain, (23) is gotten.

$$Ss_{11}(f_r,t) = Ap_r(f_r) \exp\left[j\pi K_a (t-t_d)^2\right] \exp\left[j\frac{2\pi}{3} Y_m K_a^3 (t-t_d)^3\right] \quad (23)$$

3.7. Azimuth Nonlinear Chirp Scaling Operation

After the cubic phase filtering, the azimuth nonlinear chirp scaling operation can be implemented to correct the space variance of the azimuth modulation rate. Let the ANCS function be as (24), in which $q_2(R)$ and $q_3(R)$ are undetermined.

$$H_{NCS}(t) = \exp\left(j\pi q_2(R) t^2\right) \exp\left(j\pi q_3(R) t^3\right) \quad (24)$$

Multiplying (24) with (23), the signal after ANCS operation is gotten as (25).

$$\begin{aligned} Ss_{12}(f_r, t) &= Ss_{10}(f_r, t) H_{NCS}(t) \\ &= Ap_r(f_r) \exp\left[j\pi K_a (t-t_d)^2\right] \exp\left[j\frac{2\pi}{3} Y_m K_a^3 (t-t_d)^3\right] \\ &\quad \cdot \exp\left(j\pi q_2(R) t^2\right) \exp\left(j\pi q_3(R) t^3\right) \end{aligned} \quad (25)$$

After converting (25) to the wave number domain, (26) is gotten.

$$\begin{aligned} SS_{13}(f_r,f_a) = Ap_r(f_r) &\cdot \exp\left\{-j\frac{2\pi}{K_a + q_2} f_a (f_a + K_a t_d)\right\} \\ &\cdot \exp\left\{j\frac{\pi}{(K_a+q_2)^2}\left[K_a (f_a - q_2 t_d)^2 + q_2 (f_a + K_a t_d)^2\right]\right\} \\ &\cdot \exp\left\{j\frac{\pi}{(K_a+q_2)^3}\left[\frac{2}{3} Y_m K_a^3 (f_a - q_2 t_d)^3 + q_3 (f_a + K_a t_d)^3\right]\right\} \end{aligned} \quad (26)$$

In (26) the azimuth modulation rate can be expanded with the Taylor series as (27).

$$\begin{aligned} K_a &= -\frac{2V^2 \cos^2\theta_s}{\lambda (R - V \sin\theta_s t_d)} \\ &\approx -\frac{2V^2 \cos^2\theta_s}{\lambda R} - \frac{2V^3 \cos^2\theta_s \sin\theta_s}{\lambda R^2} t_d \triangleq K_{aref} + K_{as} t_d \end{aligned} \quad (27)$$

From (26) and (27), it is found that (26) is dependent on t_d and f_a. In order to analyze the azimuth modulation rate in detail, the phase of (26) is expanded in Taylor series as (28).

$$\begin{aligned}
&\varphi_3\left(f_a, t_d\right) \\
&= \frac{1}{2!}\left[-\frac{2\pi}{K_{aref}+q_2} f_a^2 + \frac{2\pi q_2 K_{aref}}{K_{aref}+q_2} t_d^2 - 2\cdot\frac{2\pi K_{aref}}{K_{aref}+q_2} t_d f_a\right] \\
&\quad + \frac{1}{3!}\cdot 3\left[\frac{4\pi K_s K_{aref}}{\left(K_{aref}+q_2\right)^2} - \frac{4\pi K_s}{K_{aref}+q_2}\right. \\
&\quad \left. + \frac{2\pi}{\left(K_{aref}+q_2\right)^3}\left(2q_2^2 Y_m K_{aref}^3 + 3q_3 K_{aref}^2\right)\right] t_d^2 f_a \\
&\quad + \frac{1}{3!}\cdot 3\left[\frac{2\pi K_s}{\left(K_{aref}+q_2\right)^2} + \frac{2\pi}{\left(K_{aref}+q_2\right)^3}\left(-2q_2 Y_m K_{aref}^3 + 3q_3 K_{aref}\right)\right] t_d f_a^2 \\
&\quad + \frac{1}{3!}\frac{\pi\left(4Y_m K_{aref}^3 + 6q_3\right)}{\left(K_{aref}+q_2\right)^3} f_a^3 \\
&\quad + \frac{1}{3!}\left[\frac{6\pi q_2^2 K_s}{\left(K_{aref}+q_2\right)^2} + \frac{\pi K_{aref}^3}{\left(K_{aref}+q_2\right)^3}\left(-4q_2^3 Y_m + 6q_3\right)\right] t_d^3 + \ldots
\end{aligned} \tag{28}$$

In (28) only the related phase terms for determining $Y_m(R)$, $q_2(R)$ and $q_3(R)$ are left and the other terms are omitted. In order to remove the azimuth space variance of K_a, the coefficient of $t_d f_a^2$ must be zero; Moreover the azimuth position of target should not vary with t_d^2, thus the coefficient of $t_d^2 f_a$ must be zero too. The azimuth time delay of target must be t_d, thus the coefficient of $t_d f_a$ must be -2π. Here the coefficient of $t_d f_a$ is set as $-\frac{2\pi}{\alpha}$ to keep consistence with that of NCSA [9]. The α is a constant and its selection is discussed in detail in [21, 22]. So (29) is gotten.

$$\begin{cases}
\frac{K_{aref}}{K_{aref}+q_2} = \frac{1}{\alpha} \\
\frac{2K_{as}K_{aref}}{\left(K_{aref}+q_2\right)^2} - \frac{2K_{as}}{K_{aref}+q_2} + \frac{1}{\left(K_{aref}+q_2\right)^3}\left(2q_2^2 Y_m K_{aref}^3 + 3q_3 K_{aref}^2\right) = 0 \\
\frac{K_{as}}{\left(K_{aref}+q_2\right)^2} + \frac{1}{\left(K_{aref}+q_2\right)^3}\left(-2q_2 Y_m K_{aref}^3 + 3q_3 K_{aref}\right) = 0
\end{cases} \tag{29}$$

Solving (29), $Y_m(R)$, $q_2(R)$ and $q_3(R)$ can be determined as (30).

$$\begin{cases}
q_2 = \left(\alpha - 1\right) K_{aref} \\
Y_m = \frac{(\alpha - 0.5) K_{as}}{(\alpha - 1) K_{aref}^3} \\
q_3 = \frac{1}{3} K_{as}\left(\alpha - 1\right)
\end{cases} \tag{30}$$

Substituting (30) into (26), (31) is gotten.

$$SS_{13}(f_r, f_a) = Ap_r(f_r) \cdot \exp\left\{-j2\pi \frac{t_d}{\alpha} f_a\right\} \exp\left\{-j \frac{\pi}{\alpha K_{aref}} f_a^2\right\} \exp\left\{j \frac{1}{3} \frac{\pi K_{as}}{\alpha(\alpha-1) K_{aref}^3} f_a^3\right\} \exp\left\{j \frac{\pi(\alpha-1) K_{aref}}{\alpha} t_d^2\right\} \exp\left\{j \frac{\pi(\alpha-1) K_{as}}{3\alpha} t_d^3\right\} \quad (31)$$

In (31), the first exponential term gives the azimuth position of target, i.e., $\frac{t_d}{\alpha}$. The second exponential term denotes the azimuth modulation term. The azimuth modulation rate is dependent on K_{aref} and α, which means the space variance of K_a has been removed. The third exponential term is the cubic phase term that must be compensated. The forth and the fifth terms are the residual phase terms, which can be ignored.

3.8. Azimuth Compression

After ANCS operation, the azimuth compression can be implemented. The azimuth compression function is as (32).

$$H_{AC}(f_r, f_a) = \exp\left\{j \frac{\pi}{\alpha K_{aref}} f_a^2\right\} \exp\left\{-j \frac{1}{3} \frac{\pi K_{as}}{\alpha(\alpha-1) K_{aref}^3} f_a^3\right\} \quad (32)$$

After multiplying (32) with (31), (33) is gotten.

$$SS_{14}(f_r, f_a) = Ap_r(f_r) \cdot W_a(f_a) \exp\left\{-j2\pi \frac{t_d}{\alpha} f_a\right\} \quad (33)$$

All the compression steps are finished and the focusing image without geometry correction is obtained after transforming (33) to the azimuth time domain as (34).

$$SS_{15}(f_r, t) = A \sin c\left\{B_r\left[f_r + \frac{2K_r}{c}(R_0 + x_p \sin\theta_s - R_c)\right]\right\} \cdot \sin c\left\{B_a\left(t - \frac{t_d}{\alpha}\right)\right\} \quad (34)$$

3.9. Geometry Correction

From (34) it is found that after the focusing the point target position is $(R_0 + x_p \sin\theta_s, \frac{x_p}{\alpha})$. Both in range direction and in azimuth direction the image is distorted and geometry correction is necessary. After

the geometry correction, the final image can be gotten for the other applications like target identification [24, 25].

The whole processing steps of the EFSA are shown in Fig. 2.

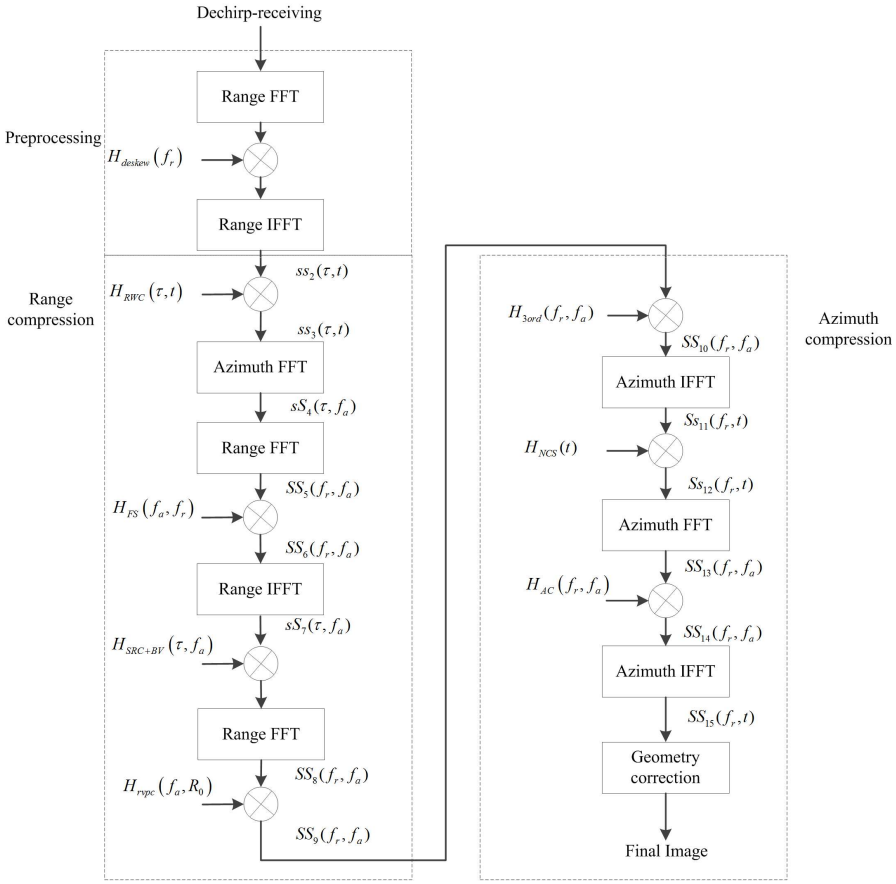

Figure 2. The processing steps of EFSA.

4. SIMULATION AND ANALYSIS

In this section, some simulation experiments based on the radar parameter settings listed in Table 1 will be given. Through the simulation results, the validity of the EFSA will be verified. And the comparison of the image quality focused by FSA, NFSA and the EFSA will be made.

Table 1. Parameter settings of high squint angle spotlight airborne SAR.

Parameter	Value	Unit	Parameter	Value	Unit
Height	5000	m	Antenna azimuth length	4	m
Velocity	100	m/s	Synthesis aperture	929	m
Carry frequency	2.7	GHz	PRF	101	Hz
Range resolution	1	m	Azimuth resolution	1.061	m
Squint angle θ_s	50	°			

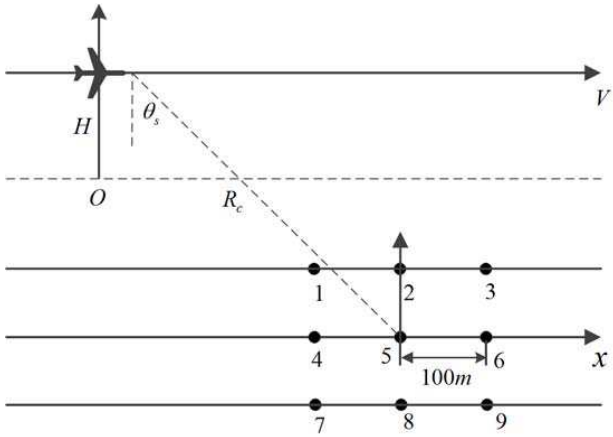

Figure 3. Scene geometry of high squint angle spotlight SAR.

According to the parameter settings in Table 1, the ideal range and azimuth resolution are 1 m × 1 m. Considering the squint angle, the ideal azimuth resolution is 1.6523 m.

The imaging scene is shown in Fig. 3. There are nine point targets in the scene. Target 5 locates at the scene center. Targets 1, 2, 3 have the same near slant range $R_n = 12200$ m; Targets 4, 5, 6 have the same center slant range $R_c = 12400$ m; And Targets 7, 8 9 have the same far slant range $R_f = 12600$ m. In the azimuth direction, targets 1, 4, 7 locate at $x_p = -100$ m; targets 2, 5, 8 locate at $x_p = 0$ m; and targets 3, 6, 9 locate at $x_p = 100$ m.

The echo signal of the scene is focused by FSA, NFSA and EFSA respectively. The image of the point target is extracted from the image of the scene and is up sampled by 4 to get the detail image. In the images of EFSA, no geometry correction is implemented. The gotten images are shown in Figs. 4–9. The corresponding calculated parameters based on the up-sampled images are all listed in Table 2.

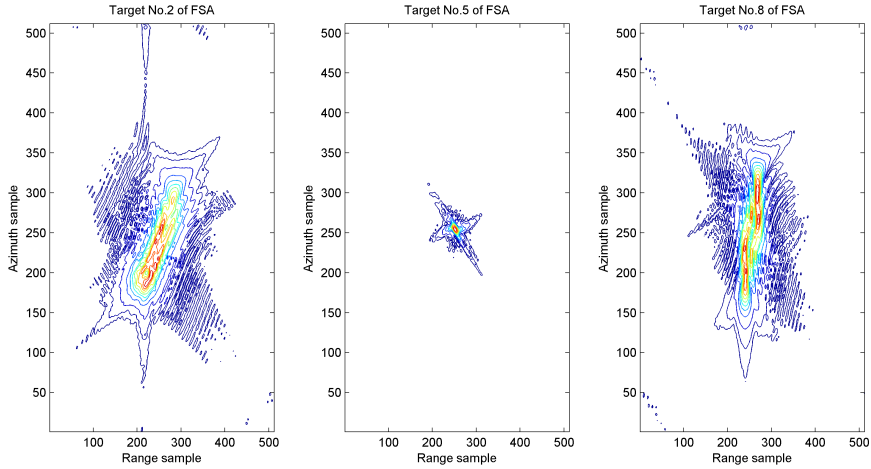

Figure 4. Images of target 2, 5, 8 gotten in FSA.

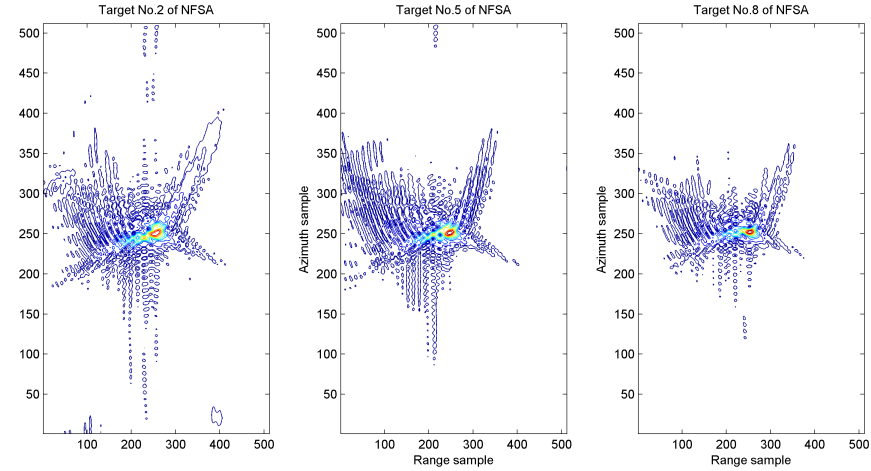

Figure 5. Images of target 2, 5, 8 gotten in NFSA.

They include range resolution, azimuth resolution, range peak sidelobe ration (PSLR), azimuth PSLR, range integrated sidelobe ration (ISLR) and azimuth ISLR.

The images focused by traditional FSA are shown in Figs. 4 and 7. It is found that the targets 4, 5, 6 with the same shortest slant range

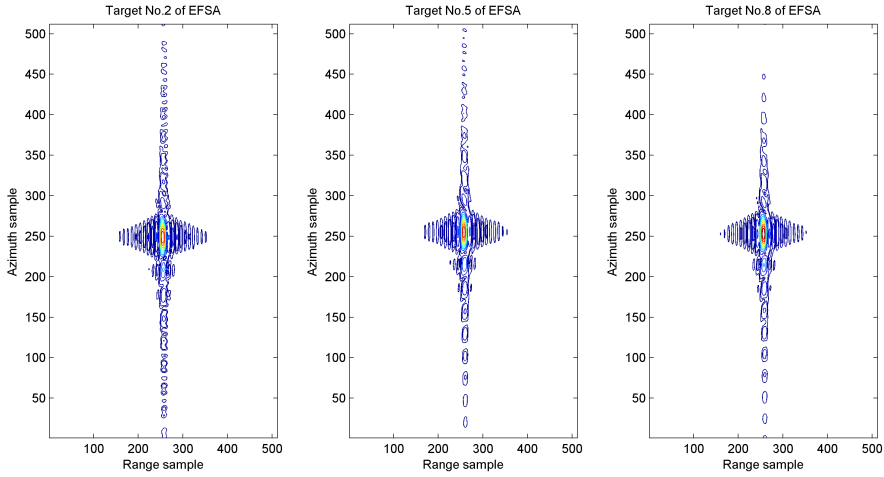

Figure 6. Images of target 2, 5, 8 gotten in the proposed method.

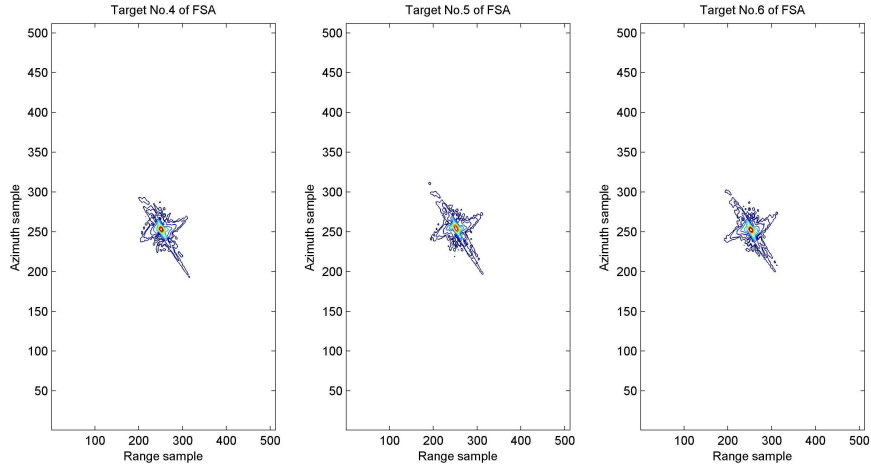

Figure 7. Images of targets 4, 5, 6 gotten in FSA.

are focused well. For the other targets, i.e., target 2 and target 8 with different shortest slant range from center target, i.e., target 5, the defocusing phenomena in range and azimuth direction are obvious. It can be explained as follows. In FSA, the echo signal is dechirp-received with a reference function whose reference slant range is the shortest range of target 5, i.e., $r_c = R_c \cos\theta_s$. Although in FSA the second

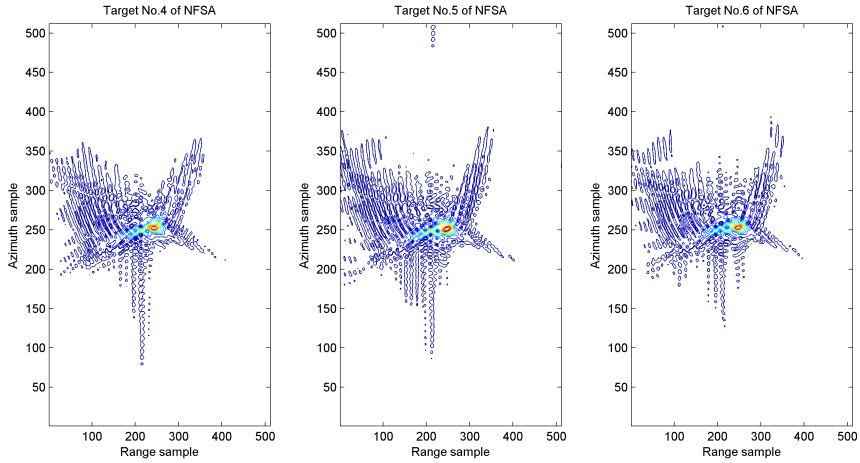

Figure 8. Images of targets 4, 5, 6 gotten in NFSA.

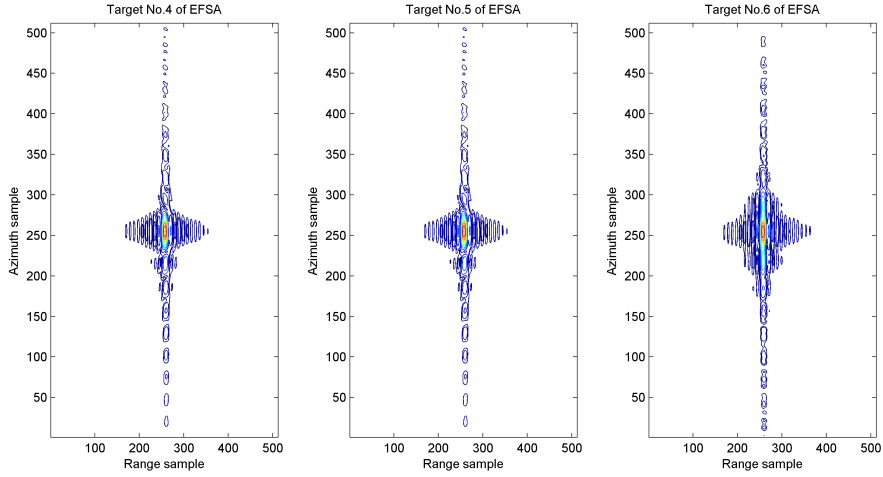

Figure 9. Images of targets 4, 5, 6 gotten in the proposed method.

range correction step neglects the space variance, this neglect will not decrease the image qualities of target 4 and 6 even with high squint angle. But for the other targets like target 2 and 8, with the high squint angle, this neglect will result in huge approximation error in the second range correction step, which will decrease the image qualities dramatically in range direction. The defocusing in range direction will further affect the azimuth focusing. This can be observed obviously in

Table 2. Calculated parameters.

Parameter		FSA	NFSA	EFSA	Parameter		FSA	NFSA	EFSA
Range Resolution (m)	T2	3.999	3.198	1.096	Azimuth PSLR (dB)	T2	–1.42	–21.1	–10.1
	T4	1.217	2.468	1.012		T4	–24.2	–22.3	–8.5
	T5	1.181	2.385	1.024		T5	–20.9	–25.5	–10.8
	T6	1.224	2.415	1.008		T6	–21.7	–8.7	–13.5
	T8	4.322	2.136	1.035		T8	–10.6	–12.7	–10.2
Azimuth Resolution (m)	T2	10.177	2.146	1.627	Range ISLR (dB)	T2	–11.0	–8.4	–10.6
	T4	1.581	1.660	1.783		T4	–7.5	–6.4	–9.3
	T5	1.898	1.693	1.540		T5	–5.8	–4.9	–9.9
	T6	1.647	1.444	1.705		T6	–6.9	–5.2	–9.5
	T8	18.165	1.282	1.465		T8	–5.9	–4.6	–10.1
Range PSLR (dB)	T2	–2.2	–7.3	–13.6	Azimuth ISLR (dB)	T2	–13.5	–9.0	–9.5
	T4	–31.5	–8.7	–12.6		T4	-12.6	–7.1	–7.5
	T5	–30.5	–6.6	–13.0		T5	–17.1	–5.5	–10.1
	T6	–31.7	–5.2	–12.6		T6	–14.1	–6.5	–5.3
	T8	-7.0	–8.7	–13.2		T8	–10.8	–8.9	–9.5

Fig. 4. The higher the squint angle is, the more serious the defocusing is.

The images focused by NFSA are shown in Figs. 5 and 8. From the diagrams and the calculated parameters shown in Table 2, it is found all the targets have the similar focusing quality. The imaging quality of the targets that are far away from the center target is improved obviously. But all the targets are not focused well especially in the range direction. The range-resolutions of all targets, including center target 5, are larger than 2 m that do not approach the ideal value 1 m.

In NFSA, the dechirp-receiving reference range is $R_c = \frac{r_c}{\cos\theta_s}$, which is different from that of FSA. The imaging quality decrease is caused by two reasons. The first one is the ignoring of the phase term whose orders are higher than 3 when extending the RD domain expression after the residual video phase removing in the preprocessing step as shown in (35). The phase error will affect the followed range compression with high squint angle. The second reason can be explained as follows. From this term $\exp\{-j\frac{2\pi r_0 \lambda K_s^2 (D(f_a)^2-1)}{c^2 D^3(f_a)}(\tau - \frac{2R_c}{c})^2\}$, it is found the range modulation rate is dependent on target shortest range r_0. In NFSA, the range modulation rate is extended at $\tau = \frac{2R_c}{c}$ and only the constant term and the 1st order term are remained. This approximation becomes

worse with the increase of the squint angle. Then the defocusing in range direction occurs in high squint angle.

$$\begin{aligned} sS(\tau, f_a) = {} & AW_a(f_a)w_r(\tau)\exp\left(-j\frac{4\pi r_0}{\lambda}\sqrt{\left(\frac{\lambda K_s}{c}\left(\tau-\frac{2R_c}{c}\right)+1\right)^2-\left(\frac{f_a\lambda}{2v}\right)^2}\right) \\ & \cdot\exp\left(j\frac{4\pi K_s R_c}{c}\left(\tau-\frac{2R_c}{c}\right)\right)\cdot\exp\left(-j\frac{2\pi x_p}{V}f_a\right) \\ \approx {} & AW_a(f_a)\,rect\left(\frac{\tau-\frac{2R_c}{c}}{T_p}\right)\cdot\exp\left\{-j\frac{4\pi r_0 D(f_a)}{\lambda}\right\}\cdot\exp\left(-j\frac{2\pi x_p}{V}f_a\right) \\ & \cdot\exp\left(-j\frac{4\pi K_s}{c}\left(\frac{r_0}{D(f_a)}-R_c\right)\left(\tau-\frac{2R_c}{c}\right)\right) \\ & \cdot\exp\left\{-j\frac{2\pi r_0\lambda K_s^2\left(D(f_a)^2-1\right)}{c^2D^3(f_a)}\left(\tau-\frac{2R_c}{c}\right)^2\right\} \\ & \cdot\exp\left\{j\frac{2\pi r_0\lambda^2 K_s^3\left(D(f_a)^2-1\right)}{c^3D^5(f_a)}\left(\tau-\frac{2R_c}{c}\right)^3\right\} \end{aligned} \tag{35}$$

The image gotten with squint angle $\theta_s = 11.508°$ by the same NFSA imaging program is shown in Fig. 10. It is found in moderate squint angle, the focusing in range direction is good.

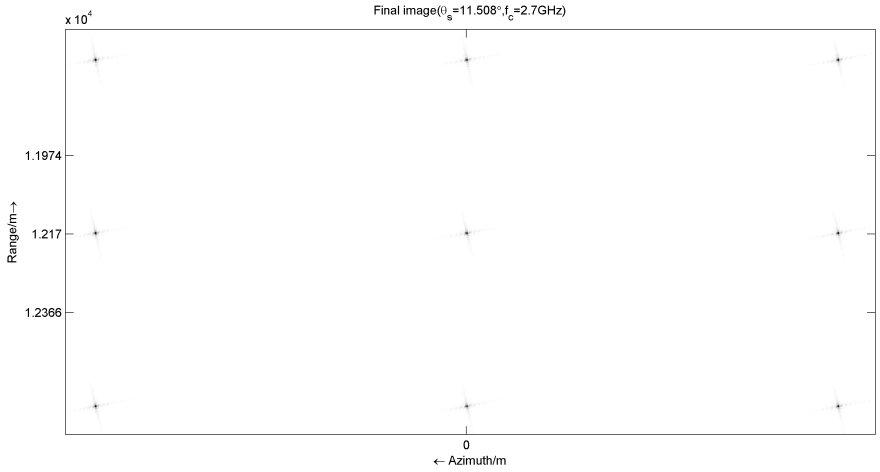

Figure 10. Image gotten in NFSA with moderate squint angle $\theta_s = 11.508°$.

The images focused by the proposed algorithm are shown in Figs. 6 and 9, from which it is found all the targets are focused much better

in contrast to FSA and NFSA. The ideal range and azimuth resolution are approached or gotten, i.e., $\rho_r = 1\,\mathrm{m}$ and $\rho_a = 1.6523\,\mathrm{m}$. This is because before the range compression, the RWC is implemented firstly. The precise compensation of the Doppler frequency center removes the serious coupling of the range and azimuth. The high squint data is converted to a broadside-like data. In the following operations, such as in FS operation, the SRC operation, although the space variance is not considered, the targets are focused well.

According to the calculated parameters list in Table 2, however, it is found the azimuth PSLR of target 4 and 6 are $-8.5\,\mathrm{dB}$ and $-13.5\,\mathrm{dB}$ respectively; the azimuth ISLR of target 4 and 6 are $-7.5\,\mathrm{dB}$ and $-5.3\,\mathrm{dB}$ respectively. We think two reasons result in the decrease of the qualities of them in azimuth direction. The first one is in (20) only the first four terms are remained. The phase approximation error will affect the azimuth focusing quality. The second one is in (27) only the constant and the 1st order term of the azimuth modulation rate are considered for the further azimuth processing. Although the performance parameters of target 4 and 6 don't approach the ideal values, their imaging qualities are improved a lot in contrast to those of FSA and NFSA. In the future research, we will concentrate on the azimuth imaging qualities improvements.

According to the previous analysis, we can conclude that the proposed method, i.e., the EFSA, is more suitable for high squint angle spotlight focusing in contrast to the traditional FSA and the NFSA. The EFSA, moreover, has the potential to be improved further.

5. CONCLUSION

In this paper a novel imaging algorithm is proposed to focus the dechirp-received data of high squint angle spotlight SAR. The RWC is implemented in 2D time domain firstly to compensate the Doppler center frequency precisely and to remove the serious coupling of the azimuth and range spectrum. The FS operation is used to get the same range migration of all the targets. The SRC, the bulk shift and the phase compensation operations finish the range compression. In the azimuth compression, because of range walk correction in 2D time domain, which results in the space variance of the azimuth modulation rate, a so-called ANCS method is involved to equalize the azimuth modulation rate. After that the azimuth compression can be finished by the azimuth phase compensation. The final image will be available after the geometry correction. The simulation experiments verify that the proposed method is more suitable for high squint angle spotlight SAR focusing than the traditional FSA and the NFSA.

ACKNOWLEDGMENT

The authors would like to thank the anonymous reviewers' suggestions to improve the quality of the paper.

REFERENCES

1. Carrara, W. G., R. S. Goodman, and R. M. Majewski, *Spotlight Synthetic Aperture Radar: Signal Processing Algorithms,* Artech House, Norwood, 1995.
2. Cantalloube, H. and P. Dubois-Fernandez, "Airborne X-band SAR imaging with 10 cm resolution: Technical challenge and preliminary results," *IEE Proc. Radar Sonar Navig.*, Vol. 152, 163–176, 2006.
3. Mittermayer, J., B. Schettler, and M. Younis, "TerraSAR-X commissioning phase execution summary," *IEEE Transactions on Geoscience and Remote Sensing*, Vol. 48, 649–659, 2010.
4. Schimpf, H., A. Wahlen, and H. Essen, "High range resolution by means of synthetic bandwidth generated by frequency-stepped chirps," *Electron. Lett.*, Vol. 39, No. 18, 1346–1348, 2003.
5. Xu, J., Y. Pi, and Z. Cao, "Bayesian compressive sensing in synthetic aperture radar imaging," *IET Radar Sonar Navig.*, Vol. 6,, No. 1, 2–8, 2012.
6. Nie, X., D. Zhu, X. Mao, and Z. Zhu, "The application of the principle of chirp scaling in processing stepped chirps in spotlight SAR," *IEEE Geoscience and Remote Sensing Letters*, Vol. 6, No. 4, 860–864, 2009.
7. Zhu, D., S. Ye, and Z. Zhu, "Polar format algorithm using chirp scaling for spotlight sar image formation," *IEEE Transactions on Aerospace and Electronic Systems*, Vol. 44, No. 4, 1433–1448, 2008.
8. Nie, X., D. Zhu, X. Mao, and Z. Zhu, "The application of the principle of chirp scaling in processing stepped chirps in spotlight SAR," *IEEE Geoscience and Remote Sensing Letters*, Vol. 6, No. 4, 860–864, 2009.
9. Shin, H.-S. and J.-T. Lim, "Range migration algorithm for airborne squint mode spotlight SAR imaging," *IET Radar Sonar Navig.*, Vol. 1, No. 1, 77–82, 2007.
10. Shin, H.-S. and J. T. Lim, "Omega-K algorithm for spaceborne spotlight SAR imaging," *IEEE Geoscience and Remote Sensing Letters*, Vol. 9, No. 3, 343–347, 2012.
11. Park, S.-H., J.-I. Park, and K.-T. Kim, "Motion compensation

for squint mode spotlight SAR imaging using efficient 2D interpolation," *Progress In Electromagnetics Research*, Vol. 128, 503–518, 2012.

12. Moreira, A., J. Mittermayer, and R. Scheiber, "Extended chirp scaling SAR data processing in stripmap, scanSAR and spotlight imaging modes," *EUSAR2000*, 749–752, Munich, Germany, Mar. 2000.
13. Lanari, R., P. Franceschetti, M. Tesauro, and E. Sansosti, "Spotlight SAR image generation based on strip mode focusing techniques," *Proc. IGARSS*, 1761–1763, Hamburg, Germany, 1999.
14. Lanari, R., M. Tesauro, E. Sansosti, and G. Fornaro, "Spotlight SAR data focusing based on a two-step processing approach," *IEEE Transactions on Geoscience and Remote Sensing*, Vol. 39, No. 9, 1993–2004, 2001.
15. An, D., X. Huang, T. Jin, and Z. Zhou, "Extended two-step focusing approach for squinted spotlight SAR imaging," *IEEE Transactions on Geoscience and Remote Sensing*, Vol. 50, No. 7, 2889–2990. 2012.
16. Mittermayer, J. and A. Moreira, "Spotlight SAR data processing using the frequency scaling algorithm," *IEEE Transactions on Geoscience and Remote Sensing*, Vol. 37, No. 5, 2198–2213, Sep. 1999.
17. Zhu, D., M. Shen, and Z. Zhu, "Some aspects of improving the frequency scaling algorithm for dechirped SAR data processing," *IEEE Transactions on Geoscience and Remote Sensing*, Vol. 46, No. 6, 1579–1588, 2008.
18. Jin, L. and X. Liu, "Nonlinear frequency scaling algorithm for high squint spotlight SAR data processing," *EURASIP Journal on Advances in Signal Processing*, Vol. 2008, 1–8, 2008.
19. Davidson, G. W., I. G. Cumming, and M. R. Ito, "A chirp scaling approach for processing squint mode SAR data," *IEEE Transactions on Aerospace and Electronic Systems*, Vol. 32, 121–133, 1996.
20. Hu, C., T. Long, and Y. Tian, "An improved nonlinear chirp scaling algorithm based on curved trajectory in geosynchronous SAR," *Progress In Electromagnetics Research*, Vol. 135, 481–513, 2013.
21. Sun, G. C., X. W. Jiang, M. D. Xing, Z. J. Qiao, Y. R. Wu, and Z. Bao, "Focus improvement of highly squinted data based on azimuth nonlinear scaling," *IEEE Transactions on Geoscience and Remote Sensing*, Vol. 49, No. 6, 2308–2322. 2011.

22. An, D. X., Z.-M. Zhou, X.-T. Huang, and T. Jin, "A novel imaging approach for high resolution squinted spotlight SAR based on the deramping-based technique and azimuth NLCS principle," *Progress In Electromagnetics Research*, Vol. 123, 485–508, 2012.
23. Wong, F. H. and T. S. Yeo, "New applications of nonlinear chirp scaling in SAR data processing," *IEEE Transactions on Geoscience and Remote Sensing*, Vol. 39, No. 5, 946–953, 2001.
24. Cao, Z. and L. Chen, "Security in application layer of radar sensor networks: Detect friends or foe," *Security and Communication Networks*, No. 1, 35–40, 2012.
25. Liao, K.-F., X.-L. Zhang, and J. Shi, "Fast 3-D microwave imaging method based on subaperture approximation," *Progress In Electromagnetics Research*, Vol. 126, 333–353, 2012.